Numerical Rebuilding of SMART-1 Plasma Plume-Spacecraft Interaction

IEPC-2005-174

Presented at the 29th International Electric Propulsion Conference, Princeton University, October 31 – November 4, 2005

A. Passaro*, A. Vicini†, F. Nania‡ and L. Biagioni§
Alta SpA, Pisa,I-56121, Italy

Abstract: This paper will present in detail the PICPluS codes, a family of simulation tools for Particle In Cell study of electric thruster plumes and interaction of the plasma field with the spacecraft. A description of the implemented physical models will be provided and will be followed by the results of the code validation against literature and experimental data. Finally, the results of the code application to the SMART-1 mission will be presented, focusing on the RPA measurement, spacecraft floating potential, and interaction of the plasma field with the satellite, in particular the solar array.

Nomenclature

n	=	number density
Id	=	discharge current
Vd	=	discharge voltage
k	=	Boltzmann constant
q	=	electron charge
T	=	temperature
ε_0	=	vacuum permeability
ρ	=	charge density
φ	=	electric potential

I. Introduction

PLASMA thrusters represent an extremely interesting technology for future space applications, but still need, at the present state knowledge, a great effort on ground characterization within proper vacuum chamber based facilities and through detailed numerical simulations. In particular, the need of simulation within realistic conditions, both for geometry and physical models, brings to the necessity of flexible 2D and 3D tools, capable to provide reasonable results in short times. During the last few years Alta SpA dedicated consistent efforts in order to individuate and develop a series of simulation instruments that can be used for design or diagnostic purposes.
This paper will describe the physical and numerical models implemented on the PICPluS (PIC Plume Simulator) code family developed at Alta SpA, in order to perform plasma thruster plume simulation and interaction with the spacecraft studies. The codes are based on the application of the Particle In Cell (PIC)[5,8] technique in the first case on a two dimensional axial symmetric grid, and in the other on a three dimensional grid. These tools were developed with the aim of implementing as many physical models as possible, in order to be able to discriminate what part of

* Project Manager, Industrial Services, a.passaro@alta-space.com.
† Senior Engineer, Industrial Services, a.vicini@alta-space.com.
‡ Aerospace Engineer, MSc, Industrial Services, f.nania@alta-space.com.
§ Chief Executive Officer, l.biagioni@alta-space.com.

the results depended on the physical or numerical assumptions; an extensive validation activity was performed considering literature data and experimental data gathered within Alta facilities.
In the framework of the Plasma Working Group created to analyze the thruster-spacecraft interaction data of ESA's SMART-1 mission, PICPluS was applied to the SMART-1 case allowing to retrieve the measured RPA data and helping explaining part of the unforeseen phenomena that were observed.

II. The PICPluS code family

A. Introduction

In this section a detailed description of the models used in the PICPluS code family, which includes a 2D and a 3D simulation program, is presented.

The PICPluS-2 code[1,3] is a two-dimensional axially-symmetric *hybrid* PIC code with Monte Carlo Collision (MCC) or Direct Simulation Monte Carlo[4] (DSMC) techniques to treat particle collisions. Several different methods to characterize important features like electron temperature are implemented, in order to be able to asses possible effects of the simulation choices on the results. In particular, a fast Successive Over Relaxation (SOR) Poisson solver is included along with the possibility to use a quasi-neutrality approach to derive plasma potential.

The PICPluS-3D code is a tri-dimensional code, originally based on a *hybrid* PIC/MCC approach, that now can also perform simple full PIC simulations with particle ions and electrons.

Both codes are based on non-uniform Cartesian structured grids with the possibility to insert solid bodies of different shapes: thanks to internal interpolation routines, different thruster units and solid bodies, that can be constituted by boxes or by *zero-thickness* lines and surfaces like planes or cylinders, can be *inserted* in the computational domain with information being passed between small dedicated grids and the main one.

1. Numerical method

Ions and neutrals

Several particle species can be independently simulated. Xenon propellant is currently used, but other propellants can be added. Background distributions of neutral propellant can be included in the simulation representing the vacuum chamber environment. Neutral atoms, possibly exiting from the thruster due to the effective ionization rate and/or from the cathode, can also be simulated (both with MCC or DSMC).

Electrons

In the hybrid approach, electrons are assumed to form a collision-less, non magnetic, and possibly isothermal fluid. The electron density is calculated by using the Boltzmann distribution (eq. 1), possibly modified in order to allow for the effect of non isothermal electron temperature T_e ($n_{e\infty}$ is chosen in order to match electron temperature measurements).

$$n_e(r,z) = n_{e\infty} e^{q\phi(r,z)/kT_e} \tag{1}$$

$$T_e(r,z) = cost \tag{2a}$$

If the isothermal fluid approach is assumed, the electron temperature is considered constant (eq. 2a). If the non isothermal option is chosen, the electron temperature can be retrieved from a simplified model using the Chapman-Enskog approach or by using the adiabatic. In the first case, considering Navier-Stokes-Fourier equations for electron fluid under stationary conditions and negligible electron drift velocity, only Laplace equation for T_e has to be solved. Retrieved electron temperature is held constant during the whole simulation allowing to compute it during the pre-processing phase. If the adiabatic approximation is used, electrons are assumed to expand as a adiabatic fluid[7,17] with temperature following eq. 2b:

$$T_e(r,z) = T_{ref}\left(\frac{n_e(r,z)}{n_{ref}}\right)^{\gamma-1} \tag{2b}$$

where $\gamma = c_p / c_V$ is a number than can be set between 5/3 (monoatomic gas) and 1, and the calculation is carried out at each time step.

Finally, in the case of full PIC model, electrons are treated as particles that can move with a different time-step than ions, in order to speed up the simulation. It has been found that, if a time step small enough for electron simulation is used also for ions, the simulation can correctly predict thruster plume fluctuations.

Potential and electric field

The electric potential can be retrieved, in the hybrid approach, after coupling to the electron component, solving the non-linear Poisson equation

$$\nabla^2\phi(r,z)+\frac{\rho_i(r,z)}{\varepsilon_0}-\frac{\rho_{e\infty}}{\varepsilon_0}e^{q\phi(r,z)/kT}=0 \tag{3}$$

which is linearized with a Newton-Raphson technique, while a relaxation technique is used to solve the linearized equation on the grid (finite differences). A Successive Over Relaxation (SOR) technique, based on checker-board ordering of updated cells is used and, in order to speed-up the relaxation, a Chebishev acceleration technique is implemented. Solution of the Poisson's equation was initially preferred to the hypothesis of plasma quasi-neutrality in the plume in order to investigate the validity of the quasi-neutrality assumption itself.
In the full 3D PIC model, the ordinary Poisson's equation is solved with an analogous SOR method or via a Multi-grid approach.
Alternatively, plasma quasi-neutrality can be imposed, deriving the electric potential from equation 1, once electron temperature and ion number density is known.

After determination of potential, the electric field is calculated using alternatively a six-point Boris scheme for the gradient on the non-uniform grid or a typical two-point scheme.

Collisions

Ion-neutral elastic and Charge Exchange (CEX) collisions can be included in the PIC cycle independently and two different collisions approaches can be chosen.

In the first one[17] (indicated as model A in the following), given an ion of velocity $\boldsymbol{v}$ and a neutral background of super-particle density n_n moving at bulk velocity $\boldsymbol{v}_n$, the frequency with which collisions occur is expressed as:

$$\nu = g\,\sigma(c_r)\,n_n, \tag{4}$$

where the relative speed is $c_r=|\boldsymbol{v}_i-\langle\boldsymbol{v}_n\rangle|$.$\sigma(c_r)$ is the sum of the elastic and CEX collisions cross sections. For charge exchange collisions these cross sections are taken to be $\sigma_{cex}=(k_1 ln(c_r)+k_2)^2\times10^{-20}$ m^2, where k_1=-0.8821 and k_2=15.1262 for single charged ions, and k_1=-2.704 and k_2=36 for double charged ions; for elastic collisions we use $\sigma_{el}=6.416\times10^{-16}$ m^2. In the case of a charge exchange the ion post collision velocity is taken either as $\boldsymbol{v}'=0.5(\boldsymbol{v}+\langle\boldsymbol{v}_n\rangle-\boldsymbol{c}_r\cdot\boldsymbol{R})$ or $\boldsymbol{v}'=\langle\boldsymbol{v}_n\rangle$ with probability 0.5 ($\boldsymbol{R}$ is a random unit vector); in the case of an elastic collision the post collision velocity is $\boldsymbol{v}'=0.5(\boldsymbol{v}+\langle\boldsymbol{v}_n\rangle+\boldsymbol{c}_r\cdot\boldsymbol{R})$. Alternatively, other cross section formulae retrieved from literature or imposed by the user can be used.
The alternative collision model here considered, indicated with model B in the following, is the induced dipole interaction by Nanbu, described in Ref.15: the collision probability of a (single-charged) ion A with molecule B within the time step Δt takes the form:

$$P_c = n_B\,(8a/\mu)^{1/2}\,\pi\,\beta_\infty^{\,2}\,\Delta t \tag{5}$$

where $a=\alpha_d e^2/[2(4\pi\varepsilon_o)^2]$, $\alpha_d/(4\pi\varepsilon_o)$ is the polarizability of the molecule, $\mu=m_A m_B/(m_A+m_B)$ is the reduced mass, and β_∞ (=9) is the cutoff of the dimensionless impact parameter

$$\beta = b(\varepsilon/4a)^{1/4} \tag{6}$$

The collision probability as expressed by (5) is constant, meaning that any molecule B is equally probable as a collision partner of ion A. A random sample of β is taken as $\beta=\beta_\infty U^{1/2}$, where U is a random number between 0 and 1. In the case of $\beta<1$ an ion is reflected on the hard-core potential, and charge-exchange occurs with probability ½. In the case of $\beta>1$ the charge-exchange probability P_{ex} is given by ½ or 0 for $\beta<\beta_{ex}(\varepsilon)$ or $\beta>\beta_{ex}(\varepsilon)$, respectively,

where $\beta_{ex}=C\varepsilon^{1/4}$. Indicating with $\boldsymbol{g}$ the relative speed between the ion and the neutral, the ion post-collision velocity when $\beta>1$ is obtained from:

$$\boldsymbol{v}' = \boldsymbol{v} \mp \tfrac{1}{2}\left[\boldsymbol{g}(1-\cos\chi) + \boldsymbol{h}\,|\sin\chi|\right] \tag{7}$$

where minus is for elastic and plus for CEX collisions; in the latter case $\boldsymbol{v}$ on the r.h.s is the neutral speed. The components of the vector $\boldsymbol{h}$ are given by:

$$\begin{aligned} h_x &= g_\perp \cos\varphi \\ h_y &= (g_x g_y \cos\varphi - g\, g_z \sin\varphi)/\, g_\perp \\ h_z &= (g_x g_z \cos\varphi - g\, g_y \sin\varphi)/\, g_\perp \end{aligned} \tag{8}$$

$g_\perp = (g_y^2+g_z^2)^{1/2}$, and the polar angle χ is tabulated as a function of the impact parameter. If $\beta<1$ the ion post-collision velocity is computed as:

$$\boldsymbol{v}' = 0.5(\boldsymbol{v} + \boldsymbol{v}_n \mp \boldsymbol{g}\,.\,\boldsymbol{R}) \tag{9}$$

where plus is for elastic and minus for CEX collisions.

Grid and time-step

The considered main physical domain is enclosed in a rectangular numerical domain in the (r,z) or (x,y,z) space. The grid is non uniform for all of the coordinates in order to adapt to the local plasma density in a simple and straightforward way; alternativily a uniform grid can be used. For what concerns boundary conditions, the domain boundary surfaces can be treated as outflows or solid walls at constant potential and temperature (standard DiRichlet or Neumann approach) with particle impacts ranging between perfect reflection and full random diffusion, with partial thermal accommodation calculated using Cercignani-Lampis-Lord model[4]; internal bodies are treated similarly.

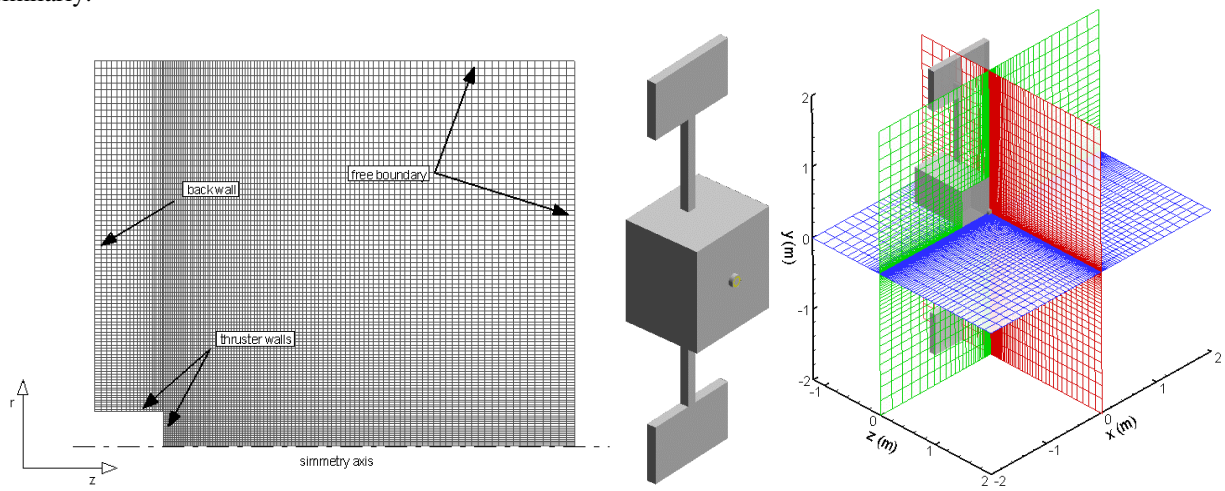

Fig. 1 Computation grids and the SMART-1 satellite model (only part of the SA simulates).

Injection data and applied magnetic field

Data regarding the particles distribution (potential, number densities, velocities) at the exit of the thruster can be provided through an input file; alternatively, different internal models can be used with the possibility to customize the distributions so as to represent the desired distributions starting from experimental or numerical data on any grid, using the code internal advanced interpolation features.
For what concerns the magnetic field, the code is realized in order to work preferentially with experimental input data: an interpolation routine can be used to adjust any input data matrix on the computational grid. If data are not available, the required fields can be automatically generated by the code through various possible models or can be set at zero level.

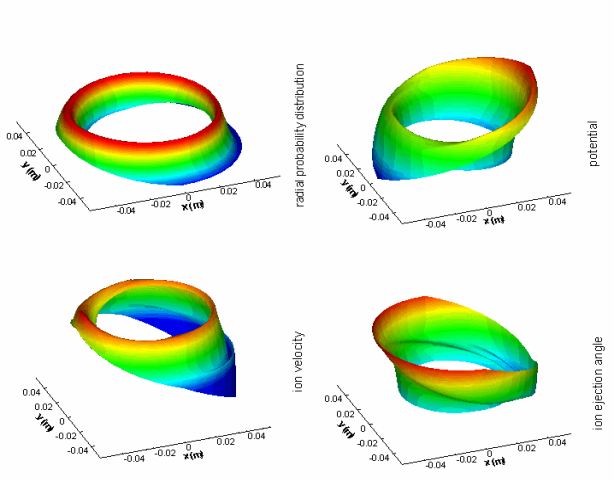

Figure 2: 3D injection probability distribution obtained from 2D simulation results for non axisymmetric inlet conditions .

2. *Code Validation*

The code results have been compared with results of similar programs and available experimental data found in the literature. In particular, five test cases were used for the Hall Effect Thrusters and and one for the Gridded Ion Engine (GIE) concept (Tab. 1). All of the test cases reached stationary conditions in about 40,000 time steps, and properties were retrieved after average over typically 1000 iterations, as indicated in Ref. 4.

Generally speaking, a good agreement was achieved for what concerns thrust, ion beam current, and ion current densities up to 90° from thruster exit. A general trend in overestimating properties on thruster axis was observed for the 2D version of the code.

Thruster Model	Vd [V]	Id [A]	Anode Mass Flow-rate [mg/s]	Background Pressure [mbar]	Ref.
SPT-100	300	4.5	4.99	$2.9\cdot10^{-6}$	
SPT-100	300	4.5	5.12	$4\cdot10^{-5}$	
SPT-100	300	4.5	5.084	$5.32\cdot10^{-5}$	
PPS-1350	350	3.47	4.21	$1\cdot10^{-4}$	
Alta XH5	350	11.16	9.2	$8.32\cdot10^{-5}$	
MUSES-C	1500	0.14	0.21	$2.0\cdot10^{-6}$	

Table 1. Test case data.

SPT-100

Data measured by King[10], Manzella[12] and Kim[9] were satisfactorily reproduced using a single set of injection conditions by both PICPluS 2 and PICPluS 3D codes as shown on Fig. 3. The difference on beam current density between 3D data and experiment at high angles is due to the long computation times needed for a three-dimensional simulation to *fill* the whole domain, in particular in the back-flow region. In fact, one of the key differences between axi-symmetric and 3D simulations seems to be due to the fact that, in order to limit the computation time and the number of simulated particles, a coarser grid is necessary for 3D simulations, forcing therefore some (limited) grid effects on the results. From a physical point of view it appears that, for an axi-symmetric simulation, slightly higher levels of

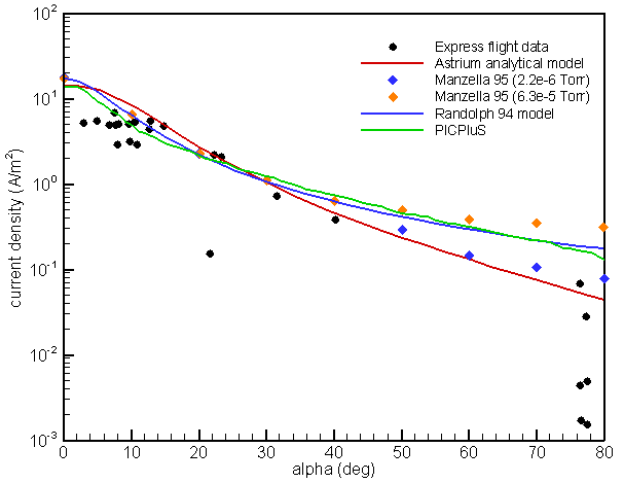

Figure 3. Comparison between 2D, 3D, and experimental data for the PPS-1350 thruster in vacuum chamber conditions.

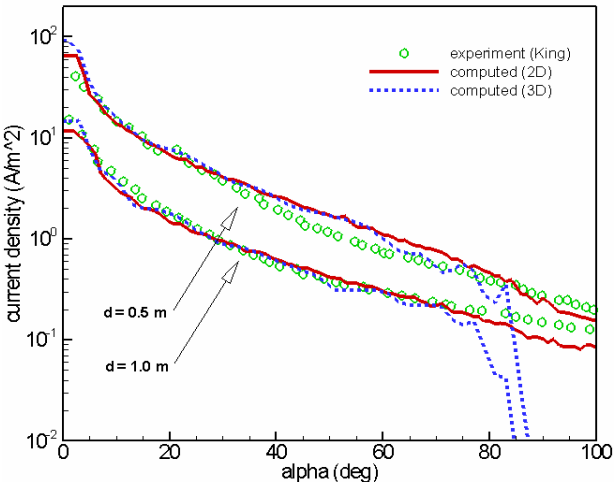

Figure 4. Comparison between 2D, 3D, and experimental data by King for the SPT-100 thruster in vacuum chamber conditions.

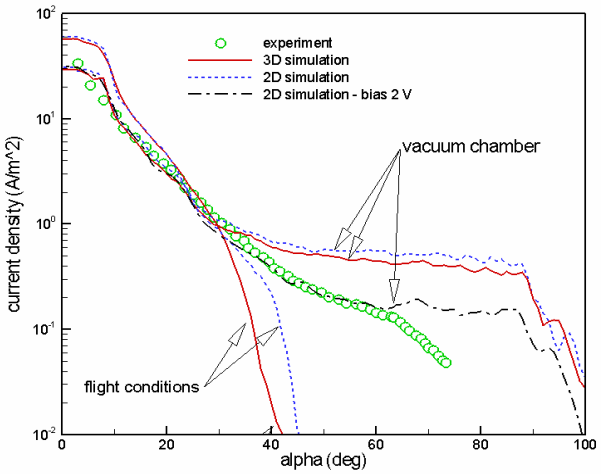

Figure 5. Comparison between 2D, 3D, and experimental data for the PPS-1350 thruster in vacuum chamber conditions.

electron temperature are obtained in the near field w.r.t to the 3D results, starting from exactly the same initial conditions.

PPS®1350

Data measured during a ground test of the PPS®1350 were made available by SNECMA for a Faraday's cup rake situated at 0.65 m from the thruster exit and run with a probe bias of some Volts. Of course, as already mentioned by Van Gilder and Boyd[19], the most important parameter determining plume behavior appears to be the inlet distributions used for ion injection: starting from the SPT-100 typical inlet distributions it was possible to identify the injection parameters able to best reproduce the experimental data, obviously including a proper probe bias, that were then used for 2D and 3D simulations. The two codes results agree fairly well (Fig. 4) for what concerns the simulation in ground conditions while a certain discrepancy (about 5 deg) can be individuated in simulation for flight conditions at angles greater than 30 deg, due to the heavy effect that, in this case, is played by the electron temperature model.

III. Comparison with flight data: SMART-1

SMART-1 is the first ESA Small Mission for Advanced Research & Technology[16], conceived to demonstrate the operation and the effectiveness of the Solar Electric Propulsion for deep space cruising in preparation of future ESA Cornerstone missions. Successfully launched on September 27th 2003, the SMART-1 satellite reached the Moon orbit on February 27th 2005 and its orbit period was extended due to a smaller than expected propellant usage up to that point. The selected strategy for the orbit raising consisted of extensive HET use for progressively expansion of the spacecraft orbit, spiralling out from the initial GTO until the spacecraft was caught by the Moon's gravitational field. The thruster fired for over 4600 hours, with the longest continuum pulse of 240 hours, obtaining a total impulse over $1 \cdot 10^6$ N[11,14]. The monitoring of the operation/environment of the EP system, during the orbit transfer from GTO to the final lunar orbit, was retained a key issue related to the SMART-1 technology objectives: for this task a specific instrument, the Electric Propulsion Diagnostic Package (EPDP), was developed by LABEN Proel Tecnologie Division (LABEN/Proel)[1313]. The EPDP operates on SMART-1 in conjunction with another instrument, SPEDE (Spacecraft Potential Electron and Dust Experiment), to achieve a comprehensive evaluation of performance and effects of the HET EP based on the PPS®1350 thruster developed by SNECMA. While the EPDP provides information on the

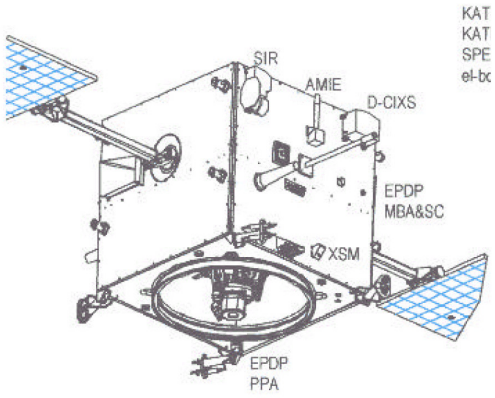

Figure 6. The SMART-1 satellite

plasma environment near the thruster, SPEDE characterizes the plasma on the spacecraft sides. The EPDP on SMART-1 is primarily intended to be operated, together with the thruster, during the spiralling escape maneuvers around the Earth, and the capture of the Moon orbit. The EPDP can be operated according to a suitable set of commands and collects information on the following areas:

– energy/current distribution of plasma ions close to the plasma beam

– plasma electronic parameters (e.g. plasma density, potential and electron temperature)

– material erosion/deposition at the Quartz Crystal Microbalance location

– Solar Cell performance (V-I measurement in open, load, short condition).

Figure 7. The LABEN/Proel EPDP unit

Mass flow rate	$4.21 \cdot 10^{-6}$ kg/s
Discharge voltage	350 V
Discharge current	3.47 A
Thrust	72.1 mN
Background pressure	$1 \cdot 10^{-9}$ Pa
Ionization efficiency	90%
Percentage of Xe^{++}	0-25%
Electron temperature model	Adiabatic or Constant
Potential field	Quasi-neutral
Potential on solid walls	0 V
Neutral atoms plume	Pre-computed

Table 2. Simulation parameters.

A. Simulation results: comparison with flight data and analysis for the RPA

A set of numerical simulations was executed with the PICPluS 3D on the grid shown in Fig. 1 considering for all of the cases the standard injection conditions shown in Table 2. The results were compared with EPDP data considering a virtual RPA probe placed in the exact EPDP location, and considering plasma features at the same place.

Looking the RPA flight data (Fig. 8) two peculiar features are evident: first of all the energy distribution presents a plateau after the primary peak with a long tail reaching energies up to 100 eV, compatible with the presence of a secondary peak situated about 20 V after the first. Secondarily, the primary peak seems to have a somewhat higher-than-expected energy while a peculiar absence of low energy impinging ions is noted.

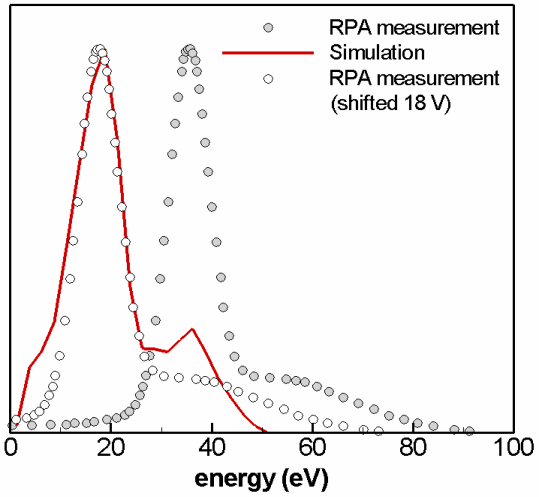

Figure 8. Comparison between numerical results and flight data for the RPA measurements.

The first set of simulations, conducted with the adiabatic model for electron temperature (with typical value of about 8 eV at the channel exit) produced a remarkably similar pattern for the RPA measurement although *shifted* by almost exactly 18 V towards lower energies. At the same time, it was noted from flight data that an almost constant gap of 18 V was present between RPA first peak position and the satellite floating potential. the explanation to this feature becomes evident considering that the RPA ground is given from the floating potential: incoming ions with energy in the plasma plume of about 18 eV are accelerated by an amount exactly equal to the floating potential by the RPA grid (summed with its sheath potential drop, that should be of some Volts) before being collected.

In any case, it was decided to extend the investigation towards two different directions: assessment of the effect of the electron temperature model and actual value on the results, and assessment of the effect of the presence of Xe^{++} ions in the flow leaving the thruster. A total of 8 numerical test cases was run with the results synthesized in the following Table 3 for the six runs concerned with the electron temperature model.

Case	T_e model	T_e Ref [eV]	Collisions model	RPA Peak 1 [V]	RPA Peak 2 [V]	Peak distance [V]	FWHM [V]	EPDP rel. pot. [V]	EPDP Te [eV]	EPDP n_i x 10^{13} [m^{-3}]
1	Adiabatic	8	Nanbu	18.8	36.1	17.3	12.9	-2.0	0.50	3.7 - 7
1b	Adiabatic	8	VHS	19.0	38.5	19.5	12.8	-2.2	0.56	3.6 – 7.2
2	Adiabatic	12	Nanbu	27.1	49.2	22.1	13.5	-5.1	1.00	7 – 9
3	Adiabatic	16	Nanbu	33.5	68.4	34.9	19.1	-5.5	1.10	5.4 – 6.8
4	Constant	3	Nanbu	26.3	43.8	17.5	11.6	-18.8	3.00	4.1
5	Constant	8	Nanbu	68.0	128.0	60.0	39.0	-50.0	8.00	3.2
EPDP flight data				**35.6**	**55**	**19.4**	**13**	**+4**	**0.62-0.72**	**6.8 – 8.7**

Table 3. Simulation results compared with EPDP data.

For what concerns the electron temperature model effect it appears that, using the adiabatic model, realistic values for T_e and ion number density are obtained in the EPDP position compared to the flight data. It can be noted that the instrument seems to lay on the edge of the plasma plume and therefore be subjected to relatively high variations of ion number density (e.g. for case 1 between $3.7 \cdot 10^{13}$ and $7 \cdot 10^{13}$ m^{-3}); the possibility of EPDP location within the plasma sheath is consistent with the fact that the EPDP individuated a slightly non-neutral plasma. The plasma potential relative to the satellite surface is always predicted as slightly negative (between -2 V and -5 V) while the corresponding measurements present always a positive value. An increase in the T_e reference value corresponds to a shift of the RPA peaks towards higher values with an overall *broadening* of the primary peak and an increasing separation of the two peaks; a significant part of low energy events is recorded in any case.

The use of a constant value for T_e produces RPA distributions which are closer to the flight data for what concerns the low energy values but usually tend to present a too high secondary peak w.r.t the first one. Electron temperature value and relative potential are extremely different from the recorded ones, while ion number density is less than expected and close to the low limits for the adiabatic cases. An increase in the temperature value produces

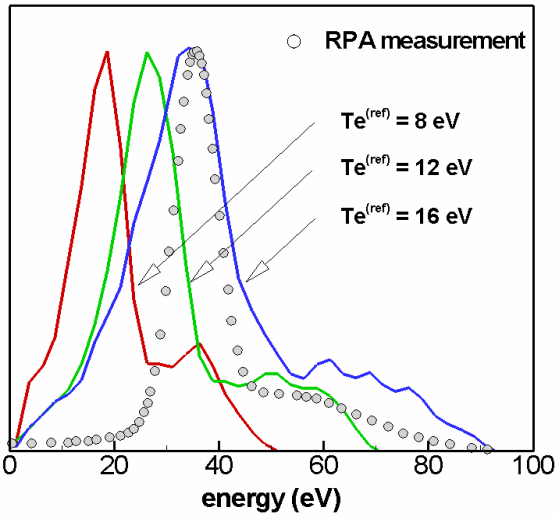

Figure 9. Effect of adiabatic model for electron temperature.

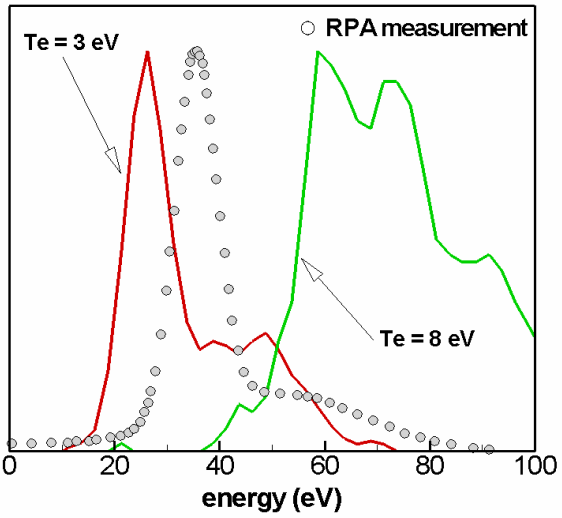

Figure 10. Effect of constant electron temperature.

a significant shift of the peaks towards higher energies (as also noted by Boyd in Ref. 6).

Considering the effects of the chosen electron temperature model on the whole plume shape (Fig. 11), one can observe that, in general, an increase of the reference T_e produces a wider plume with a stronger expansion in the axial direction. The choice of constant electron temperature tends to spread the CEX cloud that forms close to the satellite wall due to the migration of the CEX ions that are mainly generated at the exit of the acceleration channel. Nonetheless, plume shape and number density level are not extremely different in all of the considered test cases.

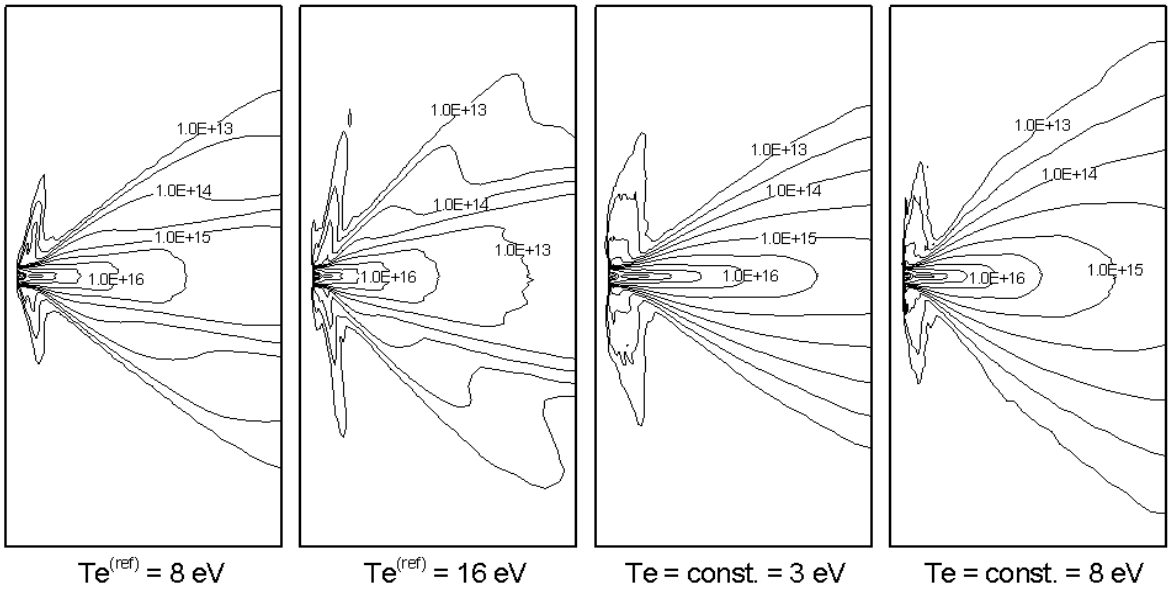

Figure 11. Comparison between computed ion number densities for test cases 1, 3, 4, and 5.

Summarizing these considerations it seems that the best way to reproduce the measured data is using the adiabatic T_e model with a reference electron temperature between 8 and 12 eV, considering the shift to be imposed on the experimental data due to the grounding at the floating potential.

The effect of the double charged ions presence is evidenced in Fig. 12 where it can be noted that, if no Xe^{++} are simulated, the RPA profile is completely different from the flight one, while a percentage of at least 20% of Xe^{++} seems needed in order to reproduce the second peak and plateau features. This is in accord with basic theoretical calculations on thruster performance, that see as necessary a similar percentage of double charged ions in order to have the prescribed discharge current, voltage and thrust. On the other hand, the possibility of charge exchange collision involving double charged ions creating fast single charged ones could imply a different percentage of starting Xe^{++} ions.

Finally, it has to be noted that, as it was likely to be expected, the simulations for flight conditions predict a higher thrust level (up to +10%) than the one measured on ground and this feature has been observed consistently within the more than 2000 hours of firing of the thruster for the orbit raising.

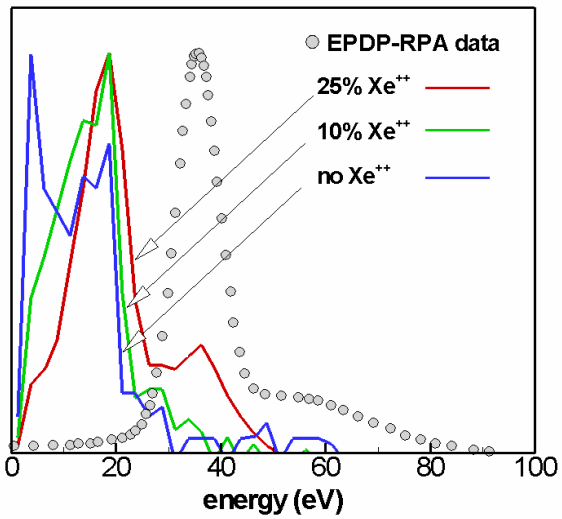

Figure 12. Comparison between numerical results and flight data for the RPA measurements.

B. Interaction with the solar array and advanced simulations.

During the whole mission, a variation of the floating potential during each orbit was found with values ranging between -5 V and +10 V approximately. The feature appeared to be consistently related to the Solar Array orientation with respect to the sun, therefore indicating a possible interaction between the SA and the thruster plume. The SA presents a front side biased to +50 V and a back side with inter-connectors that aren't shielded from the surrounding plasma. The situation was modeled with PICPluS with SA inclination angle varying by 90 deg increments.

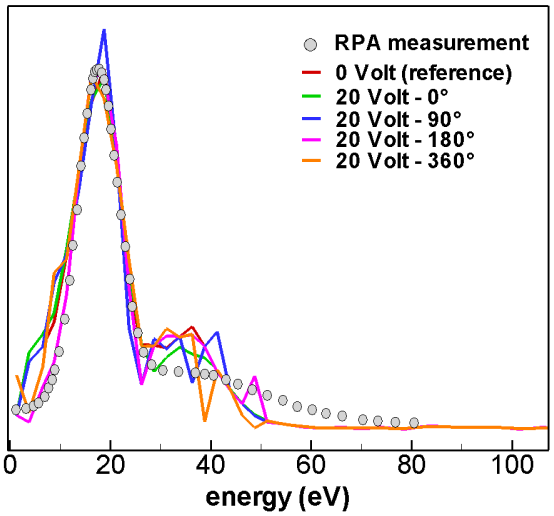

Figure 13. Comparison of the numerical results for the RPA measurements varying the SA inclination and potential distribution.

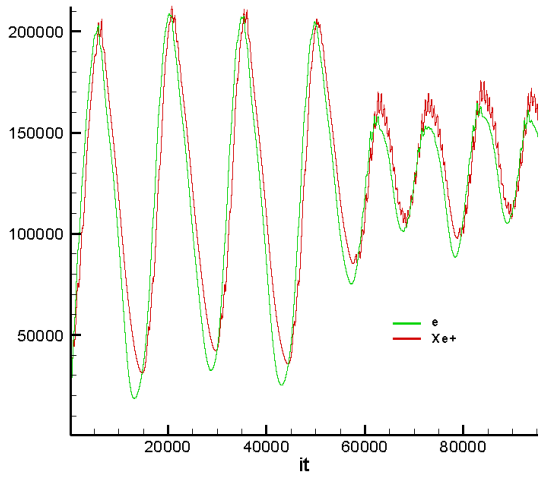

Figure 14. Fluctuations of the electron and ion population in the full 3D simulation as function of the iteration number (time step is $1 \cdot 10^{-9}$s)

The results (Fig. 13) show that, from the thruster point of view no appreciable difference in the plume is present; on the other hand, the plasma potential w.r.t. the imposed satellite potential varies with a trend similar to the measured one. A more detailed simulation is needed in order to verify quantitatively the interaction, with fine modeling of the SA elements, in order to directly retrieve the satellite floating potential.

Finally, a set of dedicated full 3D simulations was carried out as a first tentative to investigate about finer details like the plume oscillation and the non-neutral plasma individuated by the EPDP's Langmuir probe.

A very simplified configuration was run with a box representing the satellite and the thruster, with electrons and ions moving with the electron time step (around 10^{-9} s). It was found that, even considering a perfectly steady injection condition, a set of fluctuations, mainly due to ion and electron interaction involves the whole plume. Several different frequencies can be individuates ranging between some kHz and MHz (Fig. 14). Further investigation is needed in order to individuate what part of this frequencies is due to the chosen time-step and the numerics in general and what part can be considered *physical*.

It was also found out that, in the EPDP position, and in general around solid surfaces, a slightly charge imbalance is present, possibly indicating the formation of a sheath region. The satellite tends to reach a floating potential slightly negative w.r.t. the plasma potential (about -5 V) as is indicated by the EPDP data. Also in this case more work is needed in order to increase the accuracy and maturity of the simulation.

IV. Conclusion

During the last few years Alta SpA dedicated consistent efforts in order to individuate and develop a series of simulation instruments that can be used for design or diagnostic purposes. This paper focused on the PICPluS code family, illustrating at first the different physical and numerical models that are implemented in the codes. The results of the validation activity versus literature and experimental data was therefore presented. Finally, the results obtained for the SMART-1 satellite and their comparison with the in-flight data provided by the satellite instruments were presented. The RPA data was reconstructed satisfactorily and an analysis of the influence of electron temperature model and of the presence of doubly charged ions was subsequently conducted. The interaction of the thruster plume with the solar array was also investigated showing that the effects on the thruster itself are limited, while impose greater variation on the satellite, especially concerning its floating potential. A preliminary full 3D simulation was also carried out giving out indication that a completely particle simulation could be needed in order to simulate all of the phenomena experienced by the spacecraft.

Acknowledgments

The authors wish to acknowledge the help provided by Mr. Jose Gonzalez del Amo and Mr. Eric Gengembre of ESA-ESTEC as lead of the SMART-1 Plasma Working Group, Laben-PROEL for the SMART-1 in-flight data and SNECMA Moteurs for the PPS®1350 ground test data.

References

1. Andrenucci, M., Biagioni, L., Passaro, A., "PIC/DSMC Models for Hall Effect Thruster Plumes: Present Status and Ways Forward", AIAA Paper 2002-4254, July 2002.
2. Biagioni, L., Passaro, A., Andrenucci, M., "Particle Simulation of Tailored Vacuum Pumping Configurations for Electric Propulsion Testing", presented at the 4th International Symposium on Environmental Testing for Space Programmes Liege, June 2001.
3. Biagioni, L., Passaro, A., Vicini, A., "Plasma Thruster Plume Simulation: Effect of the Plasma Quasi Neutrality Hypothesis", 34th AIAA Plasmadynamics and Lasers Conference, Orlando FL , 23-26 June 2003.
4. Bird, G.A., *Molecular Gas Dynamics and the Direct Simulation of Gas Flows*, Oxford Science Publications, Oxford, 1994.
5. Birdsall, C.K., Langdon, A.B., *Plasma Physics Via Computer Simulation*, McGraw-Hill, New York, 1985.
6. Boyd, I. D., "Hall Thruster Far Field Plume Modeling and Comparison with EXPRESS Flight Data", AIAA Paper 2002-0487, 2002.
7. Celik, M., Santi, M., Cheng, S., Martinez-Sanchez, M., Peraire, J., "Hybrid-PIC Simulation of a Hall Thruster Plume on an Unstructured Grid with DSMC Collisions", presented at the 28th IEPC, Toulouse, March 2003.
8. Hockney, R.W., Eastwood, J.W., *Computer Simulation Using Particles*, McGraw-Hill, New York, 1981.
9. Kim, S. W., Foster, J. E., Gallimore, A. D., "Very Near Field Plume Study of a 1.35 kW SPT-100", AIAA Paper 96-2972, July 1996.
10. King, L.B., "Transport Property and Mass Spectral Measurements in the Plasma Exhaust Plume of a Hall Effect Space Propulsion System", Ph.D. Dissertation, Dept. Of Aerospace engineering, Univ. Of Michigan, Ann Arbor, MI, May 1998.
11. Koppel C. R., Estublier D. and all, "The SMART-1 Electric Propulsion Subsystem In Flight Experience," AIAA 2004-3435.
12. Manzella, D.H., Sankovic, J.M., "Hall Thruster Ion Beam Characterization", AIAA Paper 95-2927, July 1995.
13. Matticari, G., Noci, G., Estublier, D., Gonzales del Amo, J., Marini, A., Tajmar, M., "The Smart-1 Electric Propulsion Diagnostic Package", *Proceedings of the 3rd Spacecraft Propulsion Conference*, 2000.
14. Milligan D, Gestal D., Estublier D., Koppel C., "Smart-1 Electric Propulsion Operations", AIAA-2004-3436.
15. Nanbu, K., (2000), "Probability Theory of Electron-Molecule, Ion-Molecule, Molecule-Molecule, and Coulomb Collisions for Particle Modeling of Materials Processing Plasmas and Gases", *IEEE Transactions on Plasma Science*, Vol.28, No.3.
16. G.Racca, "An Overview of the SMART-1 Mission", 50th IAF Congress, October 1999.
17. Szabo, J.J., Fully Kinetic Numerical Modeling of a Plasma Thruster, Ph.D. Dissertation, Dept. Of Aeronautics and Astronautics, Massachussets Institute of Technology, Boston, MA, February 2001.
18. Taccogna, F., Longo, S., Capitelli, M., Particle-in-Cell with Monte Carlo Simulation of SPT-100 Exhaust Plumes, J. of Spacecraft and Rockets, Vol.39, No.3, May-June 2002.
19. Van Gilder, D.B., Boyd, I.D., "Particle Simulations of the SPT-100 Plume", AIAA Paper 98-3797, 1998.